Progress in Oceanography
May 2023, Volume 215, Pages 103034 (12p.)
https://doi.org/10.1016/j.pocean.2023.103034
https://archimer.ifremer.fr/doc/00836/94809/

Influence of combined temperature and food availability on Peruvian anchovy (*Engraulis ringens*) early life stages in the northern Humboldt Current system: A modelling approach

Flores-Valiente Jorge [1, *], Lett Christophe [2], Colas Francois [3], Pecquerie Laure [4], Aguirre-Velarde Arturo [5], Rioual Fanny [4, 5], Tam Jorge [6], Bertrand Arnaud [2], Ayón Patricia [7], Sall Saidou [8], Barrier Nicolas [2], Brochier Timothée [1]

[1] UMMISCO, Institut de Recherche pour le Développement (IRD), Sorbonne Université, Université Cheikh Anta Diop, Campus international UCAD/IRD de Hann, Dakar, Senegal
[2] MARBEC, IRD, Univ Montpellier, CNRS, Ifremer, Sète, France
[3] LOCEAN, Institut de Recherche pour le Développement (IRD), SU/IRD/CNRS/MNHN, Paris, France
[4] LEMAR, Institut de Recherche pour le Développement (IRD), UBO/IRD/CNRS/Ifremer, IUEM, Plouzané, France
[5] Laboratorio de Eco-fisiología Acuática, Instituto del Mar del Peru (IMARPE), Callao, Peru
[6] Laboratorio de Modelado Oceanográfico, Ecosistémico y del Cambio Climático (LMOECC), Instituto del Mar del Peru (IMARPE), Callao, Peru
[7] Instituto del Mar del Perú (IMARPE), Gamarra y General Valle s/n Chucuito, La Punta Callao, Peru
[8] LPAO-SF, Université Cheikh Anta Diop

* Corresponding author : Jorge Flores-Valiente, email address : jorgefloresvaliente@gmail.com

Abstract :

In the northern Humboldt Current system (NHCS), the Peruvian anchovy (Engraulis ringens) constitutes the bulk of landings and has a significant socioeconomic contribution. Understanding the impact of environment on the early-life stages of anchovy and further population dynamics remains challenging. Climate variability at a variety of scales modulates currents velocity, temperature and food availability, impacting early-life stages drift, growth and survival. In order to investigate these impacts, we developed Ichthyop-DEB, an individual-based model including larval retention processes and a Dynamic Energy Budget (DEB) bioenergetic module for larval growth. First, we assessed the effect of hydrodynamic simulations horizontal resolution on simulated larval retention patterns using a recruitment age-criterion of 30 days. Then, we evaluated the impact of the following biological processes on simulated larval recruitment patterns: i) a minimum size-criterion (2 cm), as opposed to a minimum age-criterion (30 days), to be considered as recruited, ii) the upper larval thermal limit tolerance of the species, for which lab experiments are lacking, and iii) a constant larval mortality rate. We found that using different resolutions of the hydrodynamic model (10 and 2 km) led to similar simulated larval retention patterns. Retention was highest when spawning occurred in the superficial layer (0 - 15 m) in austral winter and in the deepest considered layer (30 - 45 m) in summer. Coupling with the DEB model produced contrasted growth patterns on the continental shelf with a strong month-latitude interaction. Larval recruitment was strongest from 6° to 10° S in austral summer, largely contributing to the average seasonal pattern. Depending on the temperature correction function tested with the bioenergetic module, simulated larval recruitment

could also be strong in the northernmost zone (2° - 4°S), an area not known for abundant anchovy populations, which suggests a possible thermal growth limitation. Finally, sensitivity tests performed on larval growth limitation by food suggested a deficiency in food supply in the southernmost zone (18° - 20°S).

Highlights

► We developed an individual-based model including larval retention and a Dynamic Energy Budget bioenergetic module. ► Results show that Peruvian anchovy larval growth accelerates with increasing temperature, but the upper threshold is still not properly defined. ► Food availability limits anchovy growth and recruitment in southern Peru, only. ► Spawning depth has a significant effect on Peruvian anchovy recruitment with a seasonal modulation.

Keywords : Ichthyop-DEB model, early life stages survival, Peruvian anchovy, larval drift, larval growth

1 Introduction

The northern Humboldt Current system (NHCS) currently produces more fish catch per unit area than any other marine ecosystem (Bakun and Weeks 2008; Chavez et al. 2008) despite not having the largest primary productivity (Chavez and Messié 2009; Checkley et al. 2017). In the NHCS, the Peruvian anchovy (*Engraulis ringens*) is a highly prolific species (~15 000 eggs/batch) that reaches its sexual maturity at the age of one year. The anchovy spawns mainly in the coastal zone close to surface (Gutiérrez et al. 2007, 2008). Early life stages are taking advantage of the exceptional continental shelf nursery area thanks to the high productivity from the upwelling zone, which contribute to make *E. ringens* the most abundant species, supporting the world largest mono-specific fishery (Fréon et al. 2003; Alheit and Niquen 2004; Gutiérrez et al. 2016; Checkley et al. 2017; FAO 2020). *E. ringens* fishery is managed based on scientific monitoring of population indicators (Ayón 2000; Gutiérrez et al. 2007), but the link between environmental variability and anchovy recruitment, and thereby biomass of the adult population, is still unclear.

Modeling studies have been conducted to understand the hydrodynamics of the NHCS (Penven et al. 2005; Colas et al. 2012), its interannual variability (Colas et al. 2008; Espinoza-Morriberón et al. 2017), its potential changes under future climate scenarios (Oerder et al. 2015; Echevin et al. 2020), and the seasonal cycle and intraseasonal variability of surface chlorophyll (Echevin et al. 2008, 2014). These works provided the physical and biogeochemical basis for ecological studies in the NHCS, from testing Bakun's triad hypothesis (Bakun 1998) for small pelagic fish recruitment and early life stages survival (Lett et al. 2007) to simulating Peruvian anchovy recruitment depending on environmental conditions (Brochier et al. 2008, 2009, 2011, 2013; Xu et al. 2013, 2015).

The first anchovy larval drift modeling study conducted in the NHCS found similarities between simulated anchovy larval near surface retention over the continental shelf and observed egg distribution (Brochier et al. 2008). This results suggests a reproductive strategy of the Peruvian anchovy adapted to maximize reproduction success, a pattern also found in other Eastern Boundary Upwelling Systems (Brochier et al. 2009). Later, Brochier et al. (2013) used a physical-biogeochemical model to evaluate the effect of currents and productivity on nursery areas reduction due to climate change, and found a negative effect on Peruvian anchovy early life stages survival. However, the effects of temperature and food availability on larval growth and survival were not directly taken into account and coastal

retention was evaluated using a constant planktonic life duration (PLD) of 30 days (recruitment age-criterion). Xu et al. (2013) applied a 3D full life cycle model to the Peruvian anchovy over the period 1991 - 2007 using a bioenergetic growth model, with a 5-cm limit for the successful recruitment of individuals (recruitment size-criterion). They obtained an increased age at recruitment in 1998 (El Niño conditions) as well as a notable decrease in individuals' survival. Then, Xu et al. (2015) underlined the importance of spatial variability in environmental conditions of the NHCS and thereby on simulated recruitment of Peruvian anchovy.

Despite these previous works, the question of the relative contributions of the two main *E. ringens* spawning seasons, the most intense being in September and the second in February-March (Seatersdal and Valdivia 1964; Perea et al. 2011), to the over-all recruitment remains an open debate (Walsh et al. 1980; Perea et al. 2011). In addition, lags in spawning periods due to changes in environmental conditions have been reported (Perea and Buitrón Díaz 1999). Here we tested the hypothesis that the higher food availability combined with warmer condition in summer could contribute to better growth conditions in this season, and compensate for the lower retention pattern previously predicted in the surface layer. Such hypothesis would imply the summer spawning to be the main contribution to recruitment, which could have consequences for *E. ringens* fisheries management in Peru. In order test this hypothesis, we developed Ichthyop-DEB, an individual-based model including larval retention processes (Lett et al. 2008) and a Dynamic Energy Budget (Kooijman 2010) bioenergetic module for larval growth. Using this tool, we assessed the effect of hydrodynamic simulations horizontal resolution on simulated larval retention patterns using a recruitment age-criterion of 30 days. Then, we evaluated the impact of the following biological processes on simulated larval recruitment: i) a minimum size-criterion (2 cm), as opposed to a minimum age-criterion (30 days), to be considered as recruited, ii) the upper larval thermal limit tolerance of the species, for which lab experiments are lacking, and iii) a constant larval mortality rate.

2 Methods

An individual-based model (IBM) simulates populations and communities by following individuals and their properties (DeAngelis and Grimm 2014). Our IBM description follows the standard protocol proposed for describing IBMs (Grimm et al. 2006, 2010). Our IBM was developed from the modeling tool Ichthyop v.3.2 (Lett et al. 2008, http://www.ichthyop.org/) and since our main development is coupling with a bioenergetic growth model based on Dynamic Energy Budget (DEB) theory, hereafter we will refer to our model as Ichthyop-DEB. This new tool is able to simulate the effect of ocean currents on the drift of ichthyoplankton as well as the combined effects of temperature and food on their growth.

2.1 Purpose

The general purpose of Ichthyop-DEB is to evaluate the impact of environmental factors experienced by fish (herein anchovy) eggs and larvae on recruitment. Considered environmental factors are described in section 2.2.

2.2 Entities and state variables

The model included two types of entities: the environment and the individuals (eggs and larvae). The environment was represented by stored hydrodynamic simulations from the Coastal and Regional Ocean COmmunity model (CROCO, https://www.croco-ocean.org/, Hilt et al., 2020; Shchepetkin and McWilliams, 2005) coupled to a biogeochemical model (PISCES, Aumont et al. 2015), providing the following forcing state variables: ocean current velocities ($m\ s^{-1}$), temperature (in ºC, which will then be transformed into Kelvin degrees as a requirement of the growth model) and meso-zooplankton concentrations ($\mu mol\ C\ l^{-1}$) over the NHCS. The meso-zooplankton field was chosen as a proxy for food as it constitutes the main energy source

for anchovy larvae off Peru (Espinoza and Bertrand 2008, 2014; van der Lingen et al. 2009). In PISCES, the mesozoopankton growth equation includes a quadratic dependency to mesozooplankton in order to depict grazing by the higher, non-resolved trophic levels (Aumont et al., 2015). Individuals were characterized by the following state variables: age (d), location in 3D (longitude, latitude and depth), amount of energy reserve (E, J) and structure (V, cm^3). Structure (V) was converted to standard length using a shape coefficient (δ_M).

We used three different CROCO-PISCES configurations with contrasted grid size and bathymetry in order to evaluate the model sensitivity to spatial resolution (Table 1). The first configuration (D01) extends from 22 °S to 5 °N in latitude and from 96 °W to 70 °W in longitude, with a horizontal resolution of ~ 10 km and 64 vertical levels. The bathymetry comes from the STRM30 dataset (Becker et al. 2009). It was interpolated on the model grid and smoothed in order to reduce errors in the horizontal pressure gradient. The second configuration (D02) extends from 20 ºS to 5 ºS with a horizontal resolution of ~ 2 km and 42 vertical levels. The D02 domain is embedded into the D01 domain through an offline 1-way nesting procedure ("roms2roms"; Mason et al. 2010). We used two different bathymetries for the D02 domain, one interpolated from the D01 bathymetry (i.e., similar to the D01 bathymetry) and one interpolated directly from the SRTM30 dataset. Note that consequently the former is smoother than the latter, so in the following we call the two configurations D02s and D02r, respectively and contain no biogeochemical outputs. Horizontal advection of temperature, salinity and momentum is done with a third-order scheme (UP3), and horizontal advection of biogeochemical tracers is with a fifth-order WENO5 scheme (to avoid negative values). The vertical grid is discretized in terrain-following coordinates. The vertical advection of tracers uses a fourth-order Akima scheme and a fourth-order compact scheme, Splines, is used for the momentum vertical advection (Shchepetkin 2015). Vertical mixing is parameterized using the KPP formulation (Large et al. 1994).

The three configurations were used to obtain quasi-equilibrium solutions forced by monthly climatologies (over the period 2008-2015) at their surface and lateral boundaries. They all used the same atmospheric forcing fields. The wind stress was computed from a monthly climatology of the Advanced Scatterometer (ASCAT, 1/4° gridded product). Other atmospheric fluxes (shortwave heat fluxes and freshwater fluxes) come from the COADS monthly climatology (da Silva et al. 1994). Model sea surface temperature (SST) was restored to observed climatological monthly SST derived from the merged multi-sensor OSTIA product

(Donlon et al. 2012) following the methodology of (Barnier et al. 1995). Open boundary conditions for the D01 domain were taken from a monthly climatology of the GLORYS2V4 reanalysis (1/4° horizontal resolution; Ferry et al. 2012) for temperature, salinity, zonal and meridional current velocity components and sea-level height. Biogeochemical conditions were taken from the CARS2009 climatology (Ridgway et al. 2002) for oxygen and nutrients (nitrate, phosphate and silicate), and from the World Ocean Atlas climatology (WOA2005, Conkright et al., 2002) for dissolved organic carbon, dissolved inorganic carbon and total alkalinity. Iron is obtained from a NEMO-PISCES global simulation climatology (Aumont and Bopp 2006). Climatological simulations were run for 10 years, the first 4 years being considered as a spin-up. In the present study, the last three years were used to force Ichthyop-DEB. Note that the same D01 simulation has been used in a recent study (Echevin et al. 2021; NSH simulation therein) in which it has been shown to reproduce the general characteristics of the upwelling dynamics (and biogeochemical tracers' distribution) in the region through a validation against in-situ observations.

2.3 Process overview and scheduling

Virtual individuals (eggs/larvae) were spawned in the environment according to a determined spatial (area, depth and bathymetry) and temporal (month and frequency) spawning strategy that constituted the initial conditions (section 2.5). For each time step (2 hours) each egg or larva was passively transported by the 3D current fields, grew according to the 3D food and temperature fields and was then tested for recruitment (section 2.6).

2.4 Design concepts

Stochasticity. Individuals were initially randomly distributed over the Peruvian continental shelf. We chose the number of individuals released large enough (5 000) such that the variability of simulated recruitment between three replicates of the same simulation was negligible.

Observation. A spatio-temporal recruitment index was computed for each simulation and compared with egg presence observational data. Three recruitment criterions were tested, either based on 30-day retention over the continental shelf (criterion 1), retention until the larval length reach 2 cm (criterion 2) and mortality-weighted larval worth (see section 2.6 *mortality*) until the larval length reach 2 cm (criterion 3). Standard length of a larva used for criterion 2 and 3 relates to its structural volume (section 2.6) as follows:

$$L_w = \frac{V^{1/3}}{\delta_M} \quad \text{Eqn 1}$$

where L_w is the standard length (cm), V is the structural volume (cm^3) and δ_M is a shape coefficient.

2.5 Initialization

In each simulation, individuals were released within the coastal spawning area (Fig. 1) each month at days 1, 10 and 20, during the three climatological years used. The coastal spawning area was defined as the volume of water between latitudes 2° S and 20° S, depth range [0 – 45 m] and from the coast to isobath 2000 m. Individuals were released randomly within that defined volume, leading to a uniform distribution both horizontally and vertically.

The initial values of the bioenergetic variables for each individual were set as initial reserve $E_0 = 1J$ and initial structure $V_0 = 0.000001cm^3$. Formally, an egg is only composed of reserve but in practice a very small value for V_0 value was needed in order to avoid division by zero in the mobilization equation (Equation of the $\dot{p}_C$ flux Eqn 3, see Appendix and Kooijman 2010). We checked that a value of V_0 larger by one order of magnitude did not change the results.

2.6 Sub-models

Transport. Virtual eggs and larvae were advected using a trilinear interpolation scheme of the velocity fields derived from CROCO-PISCES, in space and time, and using a forward Euler numerical scheme with horizontal diffusion following Peliz et al. (2007). The transport was assumed to be purely Lagrangian with no egg buoyancy nor larval vertical migration.

Growth. Dynamic Energy Budget (DEB) theory (Kooijman 2010, Sousa et al. 2010) was used to simulate the growth of embryos and larvae. It describes the acquisition and utilization of energy for metabolic processes during the complete life cycle of an organism depending on temperature (T) and food conditions (X). An individual is represented by two compartments: Reserve (E, in J) and Strucuture (V, in cm^3). Energy assimilated from food in the environment contributes to reserve once the organisms starts feeding. A fraction κ of the energy mobilized from reserve is first allocated to somatic maintenance (E), and the excess energy is used to increase the structure (V), i.e., standard length (see Eqn 1). The remaining fraction of mobilized energy (1- κ) is allocated to development and maturity maintenance. The equations of the DEB model as implemented in the Lagrangian tool routines can be found in Supplementary material together with the schemes of the energy fluxes and the state variables of a DEB model for an embryo and a feeding larva. We here only present the system of two ordinary differential equations that describe the growth of an individual and how it is impacted by food (X) and temperature (T) conditions using a Holling type II scaled functional response (f) and a temperature correction function that describe how physiological rates are impacted within and outside the optimum temperature range:

$$\begin{cases} \frac{dE}{dt} = f c_T \{\dot{p}_{Am}\} V^{2/3} - \dot{p}_C \\ \frac{dV}{dt} = \frac{\kappa \dot{p}_C - c_T [\dot{p}_M] V}{[E_G]} \end{cases} \quad \text{Eqn 2}$$

$$\dot{p}_C = \frac{E\left([E_G] \frac{c_T\{\dot{p}_{Am}\}}{[E_m]} V^{-\frac{1}{3}} + [\dot{p}_M]\right)}{\kappa\left(\frac{E}{V}\right) + [E_G]} \quad \text{Eqn 3}$$

$$f = \frac{X}{(X + K)} \quad \text{Eqn 4}$$

$$c_T = exp\left(\frac{T_A}{T_1} - \frac{T_A}{T}\right)\left(\frac{1 + exp\left(\frac{T_{AL}}{T_1} - \frac{T_{AL}}{T_L}\right) + exp\left(\frac{T_{AH}}{T_H} - \frac{T_{AH}}{T_1}\right)}{1 + exp\left(\frac{T_{AL}}{T} - \frac{T_{AL}}{T_L}\right) + exp\left(\frac{T_{AH}}{T_H} - \frac{T_{AH}}{T}\right)}\right) \quad \text{Eqn 5}$$

With $[E_m]$ is the maximum reserve density and f the Holling type II scaled scaled functional response, X the local food concentration (here meso-zooplankton fields coming from CROCO-PISCES), K the half-saturation constant and C_T a non-monotonic temperature correction function, T the water temperature surrounding an individual (coming from CROCO-PISCES), T_1 is the reference temperature (for which flux parameters were estimated), T_A is the Arrhenius temperature (Kooijman 2010) and T_{AL}, T_{AH}, T_L, T_H are constants used to define a curved shape of the temperature correction according to temperature.

In the absence of observations for the Peruvian anchovy (*E. ringens*), we used here parameters estimated for the European anchovy (*Engraulis encrasicolus*, Pethybridge et al. 2013, Table 2), a taxonomically close species that is also distributed in upwelling zones. We validated that these parameters were able to describe larval growth in field and lab conditions (Figure S1).

Recruitment. We considered two criteria for larval recruitment, hereafter referred to as the age- and size-criterion, respectively. For the age-criterion, an individual was considered as recruited if it was within the coastal zone (offshore limit 2000 m isobath) at age 30 days, like in the previous modeling study (Brochier et al. 2008). For the size-criterion, an individual was considered as recruited when it was within the coastal zone at a size larger than 2 cm. The 2 cm threshold was chosen because Peruvian anchovy larvae reached an average size of 2 cm at 30 days (Castro and Hernandez 2000; Moreno et al. 2011; Rioual et al. 2021).

Mortality. We used the concept of super-individual (Scheffer et al. 1995; Parry and Evans 2008) by assigning an initial worth of 1 to each individual, then applying a constant daily mortality rate until the age at recruitment. The daily mortality rate was set to 0.1 as proposed for anchovy (Bailey and Houde 1989; Houde 2008).

2.7 Simulations and sensitivity analysis

Eight simulations were performed in order to explore the model sensitivity to different environmental forcing fields and larval growth parameters (Table 1). A first set of four simulations was carried out without the growth model, the first three (Sim 1, Sim 2 and Sim 3) in order to test the effect of the spatial resolution of the current velocity fields on simulated retention patterns using the three CROCO-PISCES configurations described in section 2.2 and

in order to fit the spatial extent of the 2 km grid, individuals release was constrained in the coastal area between 6º S and 14º S (Fig. 1, dotted box) for all three simulations. The fourth simulation (Sim 4) was similar to Sim 1, but the spawning zone was extended between 2° to 20° S aiming to compare to Brochier et al. (2008)'s results. Larval retention was calculated using an age-criterion of 30 days in all four simulations.

A second set of four simulations was carried out with the growth model, using the D01 grid and the larval size threshold (20 mm) as a criterion for recruitment (size-criterion). The DEB parameters values are given in Table 2, corresponding to *E. encrasicolus* (Pethybridge et al. 2013) but fitting *E. ringens* larval growth well (supplementary Fig. S1). In order to disentangle the effects of food and temperature on growth, and ultimately on recruitment, simulations were repeated using a half saturation parameter either null, i.e., $f = 1$ (no food limitation) or calculated such that $f = 0.5$ for the average meso-zooplankton concentration over the continental shelf off Peru with a half saturation constant of 1.6. To contrast the effect of temperature on growth, we used two different shapes for the curve of the energy fluxes temperature correction (C_T; Fig. 2). In both cases, C_T dropped to very low values for temperature higher than 25°C but in the first case the maximum value of C_T was at ~ 19 ºC and then it dropped slowly (hereafter referred to as "case 1") whereas in the second case the maximum was at ~ 23 ºC and then it dropped quickly (hereafter referred to as "case 2"). These temperature thresholds were chosen to fit *E. ringens* distribution in Peru (Castillo et al. 2022). All simulations lasted 90 days, a value found from preliminary simulations as long enough for the slowest growing individuals to reach the recruitment size. Larval retention at 30 days (age criterion, Sim 4) was also compared with the size-criterion in all four simulations (Sim 5, Sim 6, Sim 7 and Sim 8). In order to quantify the variation of results between simulations with (Sim 5, Sim 6) and without (Sim 7, Sim 8) food limitation, we calculated the percentage of variation, e.g. $\frac{Sim\,7 - Sim\,5}{Sim\,5} * 100$.

3 Results

Physical configurations

Simulated retention patterns obtained with the three tested configurations of the hydrodynamic model were very similar (Sim 1, Sim 2 and Sim3, Supplementary material, Fig. S2). The main differences concerned the D02s configuration (Sim 2) that exhibits slightly higher retention values for austral summer months (Supplementary material, Fig. S2a) and for the coastal spawning zone (0-100m isobath, Supplementary material, Fig. S2d). The latitudinal range between 10º - 12º S was the most favorable for larval retention (Supplementary material, Fig. S2b) and a direct relationship was observed between spawning depth and larval retention, being lower near the surface and higher in deeper layers (Supplementary material, Fig. S2c).

Globally, in Sim 4 we obtained similar retention patterns as Brochier et al. (2008), who used different physical forcing fields. The interaction of spawning depth and month displayed the same characteristic pattern, with highest retention in austral winter for the superficial spawning depth level (0 - 15 m) and in summer for the deepest spawning levels (30 - 45 m; bars in Fig. 3). We also found the same seasonal trends when the spawning area was split into inner shelf (0 - 100 m isobaths) and offshore shelf (100 - 500 m and 500 - 2000 m isobaths; lines in Fig. 3). The results differed most notably in highest values obtained between 8°S and 12°S from June to September in Brochier et al. (2008) as opposed to between 6°S and 8°S in January-February here (Supplementary material, Fig. S3).

Growth and bioenergetics

When we included larval growth (Sim 5 and Sim 6) and changed the criterion used for retention from age (30 days, Sim 4, grey bars in Fig. 4 and Fig. 5) to size (> 2 cm, Sim 5 and Sim 6, black line in Fig. 4 and Fig. 5) we obtained nearly identical results in temperature correction's case 2 (Sim 6, Fig. 5), i.e., when the bio-energetic fluxes decayed abruptly at high temperature.. In case 1 (Sim 5, Fig. 4), when the bio-energetic fluxes decayed smoothly at high temperature, the patterns remained similar, with highest recruitment values obtained in summer (Fig. 4a). at depth (Fig. 4c) and close to the coast (Fig. 4d). When mortality was included (red lines in Fig. 4 and Fig. 5), in case 1 the patterns did not change notably but the trends dampened (Fig. 4), whereas in case 2 (Fig. 5) we obtained a stronger seasonal variability highlighting the

difference between summer and winter (Fig. 5a) and highest values for the northern part of the domain (2º - 4º S) instead of the central (10º - 14º S) and southern (18º - 20º S) zones without mortality (Fig. 5b). Most notably, recruitment was highest for the intermediate spawning depth level (15 - 30 m) as opposed to highest for the deepest depth level (30 - 45 m) without mortality (Fig. 5c).

At the surface layer (0 - 15 m), winter spawning months favored *E. ringens* recruitment when using an age-criterion (Fig. 6a) and a size-criterion in case 1 (Fig. 6d) whereas in case 2 (Fig. 6g) recruitment tended to be uniform over months. By contrast, in intermediate layers (15 - 30 m) summer months for spawning favored recruitment when using an age-criterion (Fig. 6b) and a size-criterion in case 2 (Fig. 6h), whereas in case 1 (Fig. 6e) recruitment tended to become uniform. In deeper layers (30 - 45 m), summer favored recruitment in all cases (Fig. 6c, f, i). When mortality was included, case 1 at the surface layer (0 - 15 m, Fig. 7d) lead to fairly low and uniform recruitment whereas all other cases showed highest recruitment in summer (Fig. 7a, b, c, e, f, g, h, i).

When a size criterion was used for recruitment (criterion 2), the corresponding age at which individuals recruited was very variable, ranging from 20 to 90 days (Fig. 8). In Sim 5 (case 1), the coastal zone from 6°S to 9°S was the most favorable to early recruitment (Fig. 8a), while in Sim 6 (case 2) the northernmost zone (2-3°S) showed the lowest ages at recruitment (Fig. 8b). In case 1, recruitment started at an age of ~35 days for all spawning depth levels, and peaked at a similar age of ~50 days (Fig. 8c). In case 2, individuals in the northernmost part of the study domain recruited as early as ~20 days (Fig. 8b) and recruitment peaked at ages ~25, ~35 and ~45 days for depth levels 0 - 15, 15 - 30 and 30 - 45 m, respectively (Fig 8d).

Limitation by food

A food limitation sensitivity test between Sim 7 (case 1) and Sim 5 (case 1) showed that food acted as a growth limiting factor. This is particularly true during winter when mortality was included (Supplementary material, Fig. S4a) and in the 14º - 16° S zone (Supplementary material, Fig. S4b). Similar patterns were observed for case 2 (Sim 6 and Sim 8, Supplementary material, Fig. S5).

The amount of larvae recruiting according to their spawning location was also very variable along the coast, ranging from 0 to 150 ind/m^2 without mortality (Fig. 9a, c) and from 0 to 2 ind/m^2 cell with mortality (Fig. 9 c, d). For case 2 there were three spawning spots

favorable to recruitment in the north, center and south of the domain (Fig. 9c, d). For case 1 the northern zone was no longer favorable but the central and southern zones remained (Fig. 9a, b), which is more consistent with the spatial distribution of Peruvian anchovy egg density (eggs/m^2) derived from field surveys (Fig. 9e).

4 Discussion

We studied larval retention and growth of the Peruvian anchovy (*E. ringens*) in the northern Humboldt Current system (NHCS) using a biophysical model. This model was first forced by currents from a more modern configuration of a hydrodynamic model used previously at the same horizontal resolution (10 km; Brochier et al. 2008). We were able to replicate the general modeled patterns of larval retention obtained previously. Indeed, our results were consistent with another study aiming at answering the same scientific question but using a different dataset, thus proving the replicability of these results (*sensu* National Academies of Sciences Engineering and Medicine, 2019). This emphasis the robustness of the results despite the stochastic variability inherent to hydrodynamic model configurations. It was also crucial to replicate previous results before assessing the effects of new forcing products and other model components in order to avoid generating false conclusions (Baker 2016). Here, in particular, we found the same opposite seasonal pattern relative to spawning depth (Fig. 3) as Brochier et al. (2008). However, we obtained slightly higher coastal retention values during summer months for the three spawning depths considered. This result could be due to a greater stratification of the water column and to a higher spatial resolution of the wind stress forcing (weaker at the coast) in the new hydrodynamic simulations compared to the old one. Retention within the most coastal spawning zone (bathymetry 0 -100 m) was up to 20% higher in summer than in Brochier et al. (2008).

We then used a configuration at higher spatial resolution (2 km) and found that the simulated patterns of coastal retention remained essentially the same (Supplementary material, Fig. S1). The change in bathymetry source slightly impacted the retention values, more, in fact, than increasing the resolution. This may be due to shrinking of the continental shelf retention area in the lower resolution grid. However, these changes were too small to alter the general spatio-temporal patterns, or the general relationship between simulated retention and spawning depth or isobaths. Thus, studies focusing at the scale of the whole Peruvian continental shelf as ours can be conducted with a 10 km grid resolution without risking to miss key hydrodynamic features influencing the retention patterns. This result contrasts with previous studies, which suggested that downscaling models in coastal ecosystems may lead to significantly higher simulated retention rates (Swearer et al. 2019). However, it is in line with Vic et al. (2018) who

found stable dispersion patterns across model resolutions in the open ocean. The retention area considered here extended quite offshore with a relatively shallow continental shelf and a straight coast exposed to the open ocean, which might explain this result. Thus, despite increasing resolution might impact retention very near the coastline, the mean retention over the larger area considered here was not impacted which is in line with Garavelli et al. (2014), who showed that between 3 km and 7.5 km hydrodynamic forcings, no difference in dispersion distance was observed and both experiments also demonstrated that the closer to coast, the greater the success of the individuals. Because our results were the same between 2 and 10 km resolutions, we decided to keep the 10 km resolution in the subsequent simulations, which allowed reduced computing time of the hydrodynamic model especially when coupled to the biogeochemical module.

After including larval growth into our model based on DEB theory, we explored simulations using a size criterion for retention (Fig. 4 and Fig. 5), as opposed to an age criterion as before. Using a size criterion for retention means considering the impact of environmental variability on the planktonic life duration (PLD), which is crucial in biophysical modelling studies (Lett et al. 2010). Indeed, a shorter PLD, resulting from faster growth, is expected to increase local retention and therefore recruitment. Larvae that grow quicker may also escape predators, swim more efficiently and have therefore a better chance to survive (Houde 2008), which was also explored in our results including mortality. In our simulations, larvae experienced temperatures ranging from ~17°C in winter to ~23°C in summer. The effect of temperature on growth depended on the hypothesis we made on the C_T function (Eqn. 5) as we considered two temperature correction curves. Under the hypothesis of a max C_T at ~23.4°C (Case 1), the PLD could be as low as 20 days and the largest recruitment was found in summer in the Guayaquil Bay. However, this bay lies at the northern limit of *E. ringens* distribution (Calderón-Peralta et al. 2020), and large recruitment of Peruvian anchovy has not been observed there to our knowledge. Tuning model parameters in order to fit a known distribution is a way to study the ecological niche limits. For our model prediction to fit the spatial extent of the observed spawning area (thus excluding the Guayaquil Bay, Fig. 9e), we had to change the C_T function such that its maximum value occurs at ~19°C. In this case the average PLD of simulated recruited larvae was ~50 days, which is in the order of *in situ* and laboratory observations (Palomares et al. 1987). Furthermore, Castillo et al. (2022) showed that the main habitat temperature range of adult anchovy population was 16-24°C, which is consistent with an optimal larval growth temperature around the middle of this range. However, the hypothesis

that temperature would be the main factor limiting larval growth for individuals in the Guayaquil Bay should be challenged by new laboratory experiments designed to identify the upper temperature limit for larval growth. Indeed, current experiments found the fastest growth at 19°C for larval stages but did not investigate higher temperature values (Rioual et al. 2021). Some preliminary results tend to indicate for juvenile stages reduction of ingestion rate from 21ºC (*unpublished data*), which would impact the growth rate. So, more laboratory experiments should be designed specifically to identify the shape of the C_T function for *E. ringens*. Our results obtained with a 19°C maximum C_T (case 1) are also in line with Xu et al. (2013) who found a rather adverse effect of inter-annual variability, specifically during the El Niño period, where the number of days to reach recruitment increased and survival decreased considerably.

In simulations where food was considered as not limiting larval growth, we found similar results as in simulations where both food and temperature were limiting. This result contrasts with Thomas et al. (2016) who used a similar bio-energetic approach as ours to study oyster larvae growth and recruitment in Polynesia. In a context where temperature variability was much smaller (~28-29°C) they found that food limitation explained most of recruitment variability. In our case, larval food limitation did not impact the seasonal pattern but it had a small impact on the spatial pattern, suggesting an average higher food limitation south of the Pisco upwelling cell ($\sim 14-15$ ºS), which is in line with a lower upwelling productivity (Espinoza-Morriberón et al. 2017). Validation of simulated zooplankton fields is notoriously difficult because the corresponding data is rare. In the northern Humboldt current system off Peru, Aronés et al. (2016) studied zooplankton biomass data from 1961 to 2012 and reported a maximum biomass occurring in spring, not fully matching our simulation that predict a maximum in summer, but the data showed a considerable spatial and inter-annual variability, and the seasonal differences were strongest during the first period of the study than after. Thus, further zooplankton observations and models are needed to get a more precise idea of food limitation for larval growth in the Humboldt.

The confirmation by laboratory experiments of a “smooth” temperature correction function (as in case 1 of the present simulations) for *E. ringens* would be consistent with the widely accepted idea that temperature is a limiting factor for anchoveta blooming (Chavez et al. 2008). However, a steeper temperature correction (case 2) function would challenge this idea. In this latter case, other factors responsible for the northern limit of *E. ringens* habitat, possibly correlated with temperature, should be identified, as water masses (Bertrand et al.

2004; Swartzman et al. 2008), oxygen (Bertrand et al. 2011), or food quality (Ayón et al. 2008; Calderón-Peralta et al. 2020) as food abundance was not found as a key limiting factor in our study. The change in species dominance shown in sediment records, corresponding to periods of environmental changes (Salvatteci et al. 2018, 2019), would then be more associated to changes in stratification and circulation leading to a decrease in oxygen availability and/or decrease in ichthyoplankton retention (Brochier et al. 2013; Espinoza-Morriberón et al. 2021), affecting larval vertical distribution.

In Peru, small pelagic fish monitoring is based on spawning biomass estimation and egg and larvae surveys (Pauly and Soriano 1987; Ayón 2000; Gutiérrez et al. 2012) without explicitly accounting for spatial features (e.g. cross-shore and vertical). However, our results shows that spatial and vertical distribution also largely impact the success of recruitment. We suggest this information should be included in coupled model and observation operational system, which allows to forecast the seasonal success of recruitment. Thus, spatial monitoring of ichthyoplankton distribution should include assessment of vertical distribution. This can be achieved using multinet or, for a faster processing of the information, in situ imaging system that may allow a rapid processing (Orenstein et al. 2020).

Acknowledgments

The principal author is very grateful to the PDI (Programme Doctoral International France/Senegal) and UMMISCO (Unité Mixte de Modélisation Mathématique et Informatique des Systèmes Complexes) for their support of this research. This work is a contribution to the cooperative agreement between the Instituto del Mar del Peru (IMARPE) and the Institut de Recherche pour le Developpement (IRD) through the LMI DISCOH, JEAI DYSRUP and GDRI DEXICOTROP projects. Authors also received support from the SOLAB (Plankton interactions, their environmental determinants and biogeochemical consequences in the southern Senegal cOastal LABoratory) project, grant ANR-18-CE32-0009. Two anonymous reviewers contributed to improve the quality of this work.

Highlights

- We developed an individual-based model including larval retention and a Dynamic Energy Budget bioenergetic module.
- Results show that Peruvian anchovy larval growth accelerates with increasing temperature, but the upper threshold is still not properly defined.
- Food availability limits anchovy growth and recruitment in southern Peru, only
- Spawning depth has a significant effect on Peruvian anchovy recruitment with a seasonal modulation.

References

Alheit J, Niquen M. Regime shifts in the Humboldt Current ecosystem. Prog Oceanogr. 2004;60:201–22.

Aronés, K, Grados, D, Ayón, P, Bertrand, A. Spatio-temporal trends in zooplankton biomass in the northern Humboldt current system off Peru from 1961-2012. Deep Sea Research Part II: Topical Studies in Oceanography, Understanding changes in transitional areas of the Pacific Ocean. 2019; 169–170, 104656.

Aumont O, Bopp L. Globalizing results from ocean in situ iron fertilization studies. Global Biogeochem Cycles [Internet]. 2006 Jun 1;20(2). Available from: https://doi.org/10.1029/2005GB002591

Aumont O, Ethé C, Tagliabue A, Bopp L, Gehlen M. PISCES-v2: An ocean biogeochemical model for carbon and ecosystem studies. Geosci Model Dev. 2015;8:2465–513. https://doi.org/10.5194/gmd-8-2465-2015

Ayón P. El método de producción diaria de huevos en la estimación de labiomasa desovante del stock norte-centro de la anchoveta peruana. Boletín del Inst del Mar del Perú [Internet]. 2000;19(1–2):7–14. Available from: https://repositorio.imarpe.gob.pe/handle/20.500.12958/990

Ayón P, Swartzman G, Bertrand A, Gutiérrez M, Bertrand S. Zooplankton and forage fish species off Peru: Large-scale bottom-up forcing and local-scale depletion. Prog Oceanogr [Internet]. 2008;79(2–4):208–14. Available from: http://dx.doi.org/10.1016/j.pocean.2008.10.023

Bailey K, Houde E. Predation on Eggs and Larvae of Marine Fishes and the Recruitment Problem. Adv Mar Biol. 1989;25:1–83.

Baker M. 1,500 scientists lift the lid on reproducibility. Nature [Internet]. 2016;533(7604):452–4. Available from: https://doi.org/10.1038/533452a

Bakun A. Ocean triads and radical interdecadal variation: bane and boon to scientific fisheries management. In: Pitcher TJ, Pauly D, Hart PJB, editors. Reinventing Fisheries Management [Internet]. Dordrecht: Springer Netherlands; 1998. p. 331–58. Available from: https://doi.org/10.1007/978-94-011-4433-9_25

Bakun A, Weeks S. The marine ecosystem off Peru: What are the secrets of its fishery productivity and what might its future hold? Prog Oceanogr. 2008;79:290–9.

Barnier B, Siefridt L, Marchesiello P. Thermal forcing for a global ocean circulation model using a three-year climatology of ECMWF analyses. J Mar Syst. 1995;6:363–80.

Becker J, Sandwell D, Smith W, Braud J, Binder B, Depner J, et al. Global Bathymetry and Elevation Data at 30 Arc Seconds Resolution: SRTM30_PLUS. Mar Geod. 2009;32:355–71.

533 Bertrand A, Chaigneau A, Peraltilla S, Ledesma J, Graco M, Monetti F, et al. Oxygen: A
534 fundamental property regulating pelagic ecosystem structure in the coastal southeastern
535 tropical pacific. PLoS One. 2011;6(12):2–9.

536 Bertrand A, Segura M, Gutiérrez M, Vásquez L. From small-scale habitat loopholes to
537 decadal cycles: A habitat-based hypothesis explaining fluctuation in pelagic fish
538 populations off Peru. Fish Fish. 2004;5(4):296–316.

539 Brochier T, Colas F, Lett C, Echevin V, Cubillos L, Tam J, et al. Small pelagic fish
540 reproductive strategies in upwelling systems: A natal homing evolutionary model to
541 study environmental constraints. Prog Oceanogr [Internet]. 2009;83:261–9. Available
542 from: http://dx.doi.org/10.1016/j.pocean.2009.07.044

543 Brochier T, Echevin V, Tam J, Chaigneau A, Goubanova K, Bertrand A. Climate change
544 scenarios experiments predict a future reduction in small pelagic fish recruitment in the
545 Humboldt Current system. Glob Chang Biol. 2013;19:1841–53.

546 Brochier T, Lett C, Fréon P. Investigating the "northern Humboldt paradox" from model
547 comparisons of small pelagic fish reproductive strategies in eastern boundary upwelling
548 ecosystems. Fish Fish. 2011;12:94–109.

549 Brochier T, Lett C, Tam J, Fréon P, Colas F, Ayón P. An individual-based model study of
550 anchovy early life history in the northern Humboldt Current system. Prog Oceanogr.
551 2008;79:313–25.

552 Calderón-Peralta G, Ayora-Macias G, Solís-Coello P. Variación espacio-temporal de larvas
553 de peces en el golfo de Guayaquil, Ecuador. Boletín Investig Mar y Costeras.
554 2020;49(1):135–56.

555 Castillo PR, Peña C, Grados D, La Cruz L, Valdez C, Pozada-Herrera M, et al. Characteristics
556 of anchoveta (Engraulis ringens) schools in the optimum zone and the physiological
557 stress zone of its distribution between 2011 and 2021. Fish Oceanogr. 2022;31(5):510–
558 23.

559 Castro L, Hernandez EH. Early Life Survival of the Anchoveta Engraulis ringens Off Central
560 Chile during the 1995 and 1996 Winter Spawning Seasons. Trans Am Fish Soc.
561 2000;129:1107–17.

562 Chavez F, Bertrand A, Guevara-Carrasco R, Soler P, Csirke J. The northern Humboldt
563 Current System: Brief history, present status and a view towards the future. Prog
564 Oceanogr. 2008;79:95–105.

565 Chavez F, Messié M. A comparison of Eastern Boundary Upwelling Ecosystems. Prog
566 Oceanogr. 2009;83:80–96.

567 Checkley D, Asch R, Rykaczewski R. Climate, Anchovy, and Sardine. Ann Rev Mar Sci.
568 2017;9:469–93.

569 Colas F, Capet X, McWilliams JC, Shchepetkin A. 1997-1998 El Niño off Peru: A numerical
570 study. Prog Oceanogr. 2008;79:138–55.

571 Colas F, McWilliams JC, Capet X, Kurian J. Heat balance and eddies in the Peru-Chile

572 current system. Clim Dyn. 2012;39:509–29.

573 Conkright ME, Locarnini RA, Garcia HE, O'Brien TD, Boyer TP, Stephens C, et al. World
574 Ocean Atlas 2001: Objective analyses, data statistics, and figures [CD-ROM]. 2002;

575 DeAngelis DL, Grimm V. Individual-based models in ecology after four decades.
576 F1000Prime Rep. 2014;6(June).

577 Donlon C, Martin M, Stark J, Roberts-Jones J, Fiedler E, Wimmer W. The Operational Sea
578 Surface Temperature and Sea Ice Analysis (OSTIA) system. Remote Sens Environ.
579 2012;116:140–58.

580 Echevin V, Albert A, Lévy M, Graco M, Aumont O, Piétri A, et al. Intraseasonal variability
581 of nearshore productivity in the Northern Humboldt Current System: The role of coastal
582 trapped waves. Cont Shelf Res [Internet]. 2014;73:14–30. Available from:
583 http://dx.doi.org/10.1016/j.csr.2013.11.015

584 Echevin V, Aumont O, Ledesma J, Flores G. The seasonal cycle of surface chlorophyll in the
585 Peruvian upwelling system: A modelling study. Prog Oceanogr [Internet]. 2008;79:167–
586 76. Available from: http://dx.doi.org/10.1016/j.pocean.2008.10.026

587 Echevin V, Gévaudan M, Espinoza-Morriberón D, Tam J, Aumont O, Gutierrez D, et al.
588 Physical and biogeochemical impacts of RCP8.5 scenario in the Peru upwelling system.
589 Biogeosciences. 2020;17:3317–41.

590 Echevin, V, Hauschildt, J, Colas, F, Thomsen, S, & Aumont, O. Impact of chlorophyll
591 shading on the Peruvian upwelling system. Geophysical Research Letters. 2021; *48*(19),
592 e2021GL094429.

593 Espinoza-Morriberón D, Echevin V, Colas F, Tam J, Ledesma J, Vasquez L, et al. Impacts of
594 El Niño events on the Peruvian upwelling system productivity. J Geophys Res Ocean.
595 2017;122:5423–44.

596 Espinoza-Morriberón D, Echevin V, Gutiérrez D, Tam J, Graco M, Ledesma J, et al.
597 Evidences and drivers of ocean deoxygenation off Peru over recent past decades. Vol.
598 11, Scientific Reports. 2021.

599 Espinoza P, Bertrand A. Revisiting Peruvian anchovy (Engraulis ringens) trophodynamics
600 provides a new vision of the Humboldt Current system. Prog Oceanogr. 2008;79:215–27.

601 Espinoza P, Bertrand A. Ontogenetic and spatiotemporal variability in anchoveta Engraulis
602 ringens diet off Peru. J Fish Biol. 2014;422–35.

603 FAO. The State of World Fisheries and Aquaculture. Rome; 2020.

604 Ferry N, Parent L, Garric G, Bricaud C, Testut C, Le Galloudec O, et al. GLORYS2V1 global
605 ocean reanalysis of the altimetric era (1992–2009) at meso scale. Mercat Ocean Newsl.
606 2012;44.

607 Fréon P, Mullon C, Voisin B. Investigating remote synchronous patterns in fisheries. Fish
608 Oceanogr. 2003;12(4–5):443–57.

609 Garavelli L, Kaplan DM, Colas F, Stotz W, Yannicelli B, Lett C. Identifying appropriate
610 spatial scales for marine conservation and management using a larval dispersal model:
611 The case of Concholepas concholepas (loco) in Chile. Prog Oceanogr [Internet].
612 2014;124:42–53. Available from: http://dx.doi.org/10.1016/j.pocean.2014.03.011

613 Grimm V, Berger U, Bastiansen F, Eliassen S, Ginot V, Giske J, et al. A standard protocol for
614 describing individual-based and agent-based models. Ecol Modell. 2006;198:115–26.

615 Grimm V, Berger U, DeAngelis D, Polhill JG, Giske J, Railsback SF. The ODD protocol: A
616 review and first update. Ecol Modell. 2010;221:2760–8.

617 Gutiérrez D, Akester M, Naranjo L. Productivity and sustainable management of the
618 Humboldt current large marine ecosystem under climate change. Environ Dev.
619 2016;17:126–44.

620 Gutiérrez M, Castillo R, Segura M, Peraltilla S, Flores M. Trends in spatio-temporal
621 distribution of Peruvian anchovy and other small pelagic fish biomass from 1966-2009.
622 Lat Am J Aquat Res [Internet]. 2012;40:633–48. Available from:
623 http://lajar.ucv.cl/index.php/rlajar/article/view/vol40-issue3-fulltext-12

624 Gutiérrez M, Dordon S, Bertrand A, Bertrand S. Anchovy (Engraulis ringens) and sardine
625 (Sardinops sagax) spatial dynamics and aggregation patterns in the Humboldt Current
626 ecosystem, Peru, from 1983-2003. Fish Oceanogr. 2007;16(2):155–68.

627 Gutiérrez M, Ramirez A, Bertrand S, Móron O, Bertrand A. Ecological niches and areas of
628 overlap of the squat lobster "munida" (Pleuroncodes monodon) and anchoveta (Engraulis
629 ringens) off Peru. Prog Oceanogr [Internet]. 2008;79(2–4):256–63. Available from:
630 http://dx.doi.org/10.1016/j.pocean.2008.10.019

631 Hilt M, Auclair F, Benshila R, Bordois L, Capet X, Debreu L, et al. Numerical modelling of
632 hydraulic control, solitary waves and primary instabilities in the Strait of Gibraltar.
633 Ocean Model. 2020;151:1–16.

634 Houde E. Emerging from Hjort's shadow. J Northwest Atl Fish Sci. 2008;41:53–70.

635 Kooijman SALM. Dynamic Energy Budget Theory for Metabolic Organisation [Internet]. 3rd
636 ed. Cambridge: Cambridge University Press; 2010. Available from:
637 https://www.cambridge.org/core/books/dynamic-energy-budget-theory-for-metabolic-
638 organisation/A50EC7C47CEAEE4100A24BE0DAD537DB

639 Large, W G, McWilliams, J C, & Doney, S C. Oceanic vertical mixing: A review and a model
640 with a nonlocal boundary layer parameterization. *Reviews of geophysics*. 1994; *32*(4),
641 363-403.

642 Lett C, Ayata SD, Huret M, Irisson JO. Biophysical modelling to investigate the effects of
643 climate change on marine population dispersal and connectivity. Prog Oceanogr
644 [Internet]. 2010;87(1–4):106–13. Available from:
645 http://dx.doi.org/10.1016/j.pocean.2010.09.005

646 Lett C, Penven P, Ayón P, Fréon P. Enrichment, concentration and retention processes in
647 relation to anchovy (Engraulis ringens) eggs and larvae distributions in the northern
648 Humboldt upwelling ecosystem. J Mar Syst. 2007;64:189–200.

649 Lett C, Verley P, Mullon C, Parada C, Brochier T, Penven P, et al. A Lagrangian tool for
650 modelling ichthyoplankton dynamics. Environ Model Softw. 2008;23:1210–4.

651 Mason E, Molemaker J, Shchepetkin AF, Colas F, McWilliams JC, Sangrà P. Procedures for
652 offline grid nesting in regional ocean models. Ocean Model. 2010;35:1–15.

653 Moreno P, Claramunt G, Castro L. Transition period from larva to juvenile in anchoveta
654 Engraulis ringens. Length or age related? J Fish Biol. 2011;78:825–37.

655 National Academies of Sciences Engineering and Medicine. Reproducibility and Replicability
656 in Science [Internet]. Washington, DC: The National Academies Press; 2019. Available
657 from: https://nap.nationalacademies.org/catalog/25303/reproducibility-and-replicability-
658 in-science

659 Oerder V, Colas F, Echevin V, Codron F, Tam J, Belmadani A. Peru-Chile upwelling
660 dynamics under climate change. J Geophys Res Ocean. 2015;120:1152–72.

661 Orenstein EC, Ratelle D, Briseño-Avena C, Carter ML, Franks PJS, Jaffe JS, et al. The
662 Scripps Plankton Camera system: A framework and platform for in situ microscopy.
663 Limnol Oceanogr Methods [Internet]. 2020 Nov 1;18(11):681–95. Available from:
664 https://doi.org/10.1002/lom3.10394

665 Palomares D, Muck P, Mendo J, Chuman E, Gomez O, Pauly D. Growth of the Peruvian
666 Anchovy (Engraulis ringens), 1953 to 1982. In: Pauly D, Tsukuyama I, editors. The
667 Peruvian anchoveta and its upwelling ecosystem: three decades of change. 1987. p. 117–
668 41.

669 Parry HR, Evans AJ. A comparative analysis of parallel processing and super-individual
670 methods for improving the computational performance of a large individual-based
671 model. Ecol Modell. 2008;214:141–52.

672 Pauly D, Soriano M. Monthly spawning stock and egg production of Peruvian anchoveta
673 (Engraulis ringens), 1953 to 1982. In: Pauly D, Tsukayama I, editors. The Peruvian
674 anchoveta and its upwelling ecosystem: three decades of change. 1987. p. 167–78.

675 Peliz A, Marchesiello P, Dubert J, Marta-Almeida M, Roy C, Queiroga H. A study of crab
676 larvae dispersal on the Western Iberian Shelf: Physical processes. J Mar Syst.
677 2007;68:215–36.

678 Penven P, Echevin V, Pasapera J, Colas F, Tam J. Average circulation, seasonal cycle, and
679 mesoscale dynamics of the Peru Current System: A modeling approach. J Geophys Res
680 C Ocean. 2005;110:1–21.

681 Perea Á, Buitrón Díaz B. Condición reproductiva de Engraulis ringens y Vinciguerria lucetia
682 pacifici en el mar peruano durante la primavera 1998. 1999;

683 Perea Á, Peña C, Oliveros-Ramos R, Buitrón B, Mori J. Potential egg production,
684 recruitment, and closed fishing season of the Peruvian anchovy (Engraulis ringens):
685 Implications for fisheries management. Ciencias Mar. 2011;37:585–601.

686 Pethybridge H, Roos D, Loizeau V, Pecquerie L, Bacher C. Responses of European anchovy
687 vital rates and population growth to environmental fluctuations: An individual-based

688 modeling approach. Ecol Modell [Internet]. 2013;250:370–83. Available from:
689 http://dx.doi.org/10.1016/j.ecolmodel.2012.11.017

690 Ridgway KR, Dunn JR, Wilkin JL. Ocean Interpolation by Four-Dimensional Weighted Least
691 Squares—Application to the Waters around Australasia. J Atmos Ocean Technol
692 [Internet]. 2002;19(9):1357–75. Available from:
693 https://journals.ametsoc.org/view/journals/atot/19/9/1520-
694 0426_2002_019_1357_oibfdw_2_0_co_2.xml

695 Rioual F, Ofelio C, Rosado-Salazar M, Dionicio-Acedo J, Peck MA, Aguirre-Velarde A.
696 Embryonic development and effect of temperature on larval growth of the Peruvian
697 anchovy Engraulis ringens. J Fish Biol. 2021;(April):1–18.

698 Salvatteci R, Field D, Gutiérrez D, Baumgartner T, Ferreira V, Ortlieb L, et al. Multifarious
699 anchovy and sardine regimes in the Humboldt Current System during the last 150 years.
700 Glob Chang Biol. 2018;24(3):1055–68.

701 Salvatteci R, Gutierrez D, Field D, Sifeddine A, Ortlieb L, Caquineau S, et al. Fish debris in
702 sediments from the last 25 kyr in the Humboldt Current reveal the role of productivity
703 and oxygen on small pelagic fishes. Prog Oceanogr [Internet]. 2019;176(May):102114.
704 Available from: https://doi.org/10.1016/j.pocean.2019.05.006

705 Scheffer M, Baveco J, DeAngelis D, Rose K, van Nes E. Super-individuals a simple solution
706 for modelling large populations on an individual basis. Ecol Modell. 1995;80:161–70.

707 Seatersdal G, Valdivia J. Un estudio del crecimiento, tamaño y reclutamiento de la anchoveta
708 (*Engraulis ringens*) Basado en datos de frecuencia de longitud. 1964;

709 Shchepetkin AF, McWilliams JC. The regional oceanic modeling system (ROMS): A split-
710 explicit, free-surface, topography-following-coordinate oceanic model. Ocean Model.
711 2005;9:347–404.

712 Shchepetkin, AF. An adaptive, Courant-number-dependent implicit scheme for vertical
713 advection in oceanic modeling. Ocean Model. 2015; *91*, 38-69.

714 da Silva AM, Young CC, Levitus S. Atlas of surface marine data 1994, Vol. 1: Algorithms
715 and procedures. Noaa atlas nesdis. 1994;6(83):20910–3282.

716 Sousa T, Domingos T, Poggiale J-C, Kooijman SALM. Formalised DEB theory restores
717 coherence in core biology. Phil. Trans. R. Soc. Lond. B Biol. Sci. 2010 ; **365**, 3433--
718 3428.

719 Swartzman G, Bertrand A, Gutiérrez M, Bertrand S, Vasquez L. The relationship of anchovy
720 and sardine to water masses in the Peruvian Humboldt Current System from 1983 to
721 2005. Prog Oceanogr. 2008;79(2–4):228–37.

722 Swearer SE, Treml EA, Shima JS. A review of biophysical models of marine larval dispersal.
723 CRC Press; 2019.

724 Thomas Y, Dumas F, Andréfouët S. Larval connectivity of pearl oyster through biophysical
725 modelling; evidence of food limitation and broodstock effect. Estuar Coast Shelf Sci.
726 2016;182:283–93.

van der Lingen, C.D., Bertrand, A., Bode, A., Brodeur, R., Cubillos, L., Espinoza, P., Friedland, K., Garrido, S., Irigoien, X., Miller, T., Möllmann, C., Rodriguez-Sanchez, R., Tanaka, H., Temming, A., 2009. Trophic dynamics, in: Roy, C., Checkley, D., Alheit, J., Oozeki, Y. (Eds.), Climate Change and Small Pelagic Fish. Cambridge University Press, Cambridge, pp. 112–157.

Vic C, Gula J, Roullet G, Pradillon F. Dispersion of deep-sea hydrothermal vent effluents and larvae by submesoscale and tidal currents. Deep Res Part I Oceanogr Res Pap [Internet]. 2018;133(January):1–18. Available from: https://doi.org/10.1016/j.dsr.2018.01.001

Walsh JJ, Whitledge TE, Esaias WE, Smith RL, Huntsman SA, Santander H, et al. The spawning habitat of the Peruvian anchovy, Engraulis ringens. Deep Sea Res Part A, Oceanogr Res Pap. 1980;27(1):1–27.

Xu Y, Chai F, Rose KA, Ñiquen C. M, Chavez FP. Environmental influences on the interannual variation and spatial distribution of Peruvian anchovy (Engraulis ringens) population dynamics from 1991 to 2007: A three-dimensional modeling study. Ecol Modell. 2013;264:64–82.

Xu Y, Rose KA, Chai F, Chavez FP, Ayón P. Does spatial variation in environmental conditions affect recruitment? A study using a 3-D model of Peruvian anchovy. Prog Oceanogr. 2015;138:417–30.

Highlights

- We developed an individual-based model including larval retention and a Dynamic Energy Budget bioenergetic module.
- Results show that Peruvian anchovy larval growth accelerates with increasing temperature, but the upper threshold is still not properly defined.
- Food availability limits anchovy growth and recruitment in southern Peru, only
- Spawning depth has a significant effect on Peruvian anchovy recruitment with a seasonal modulation.

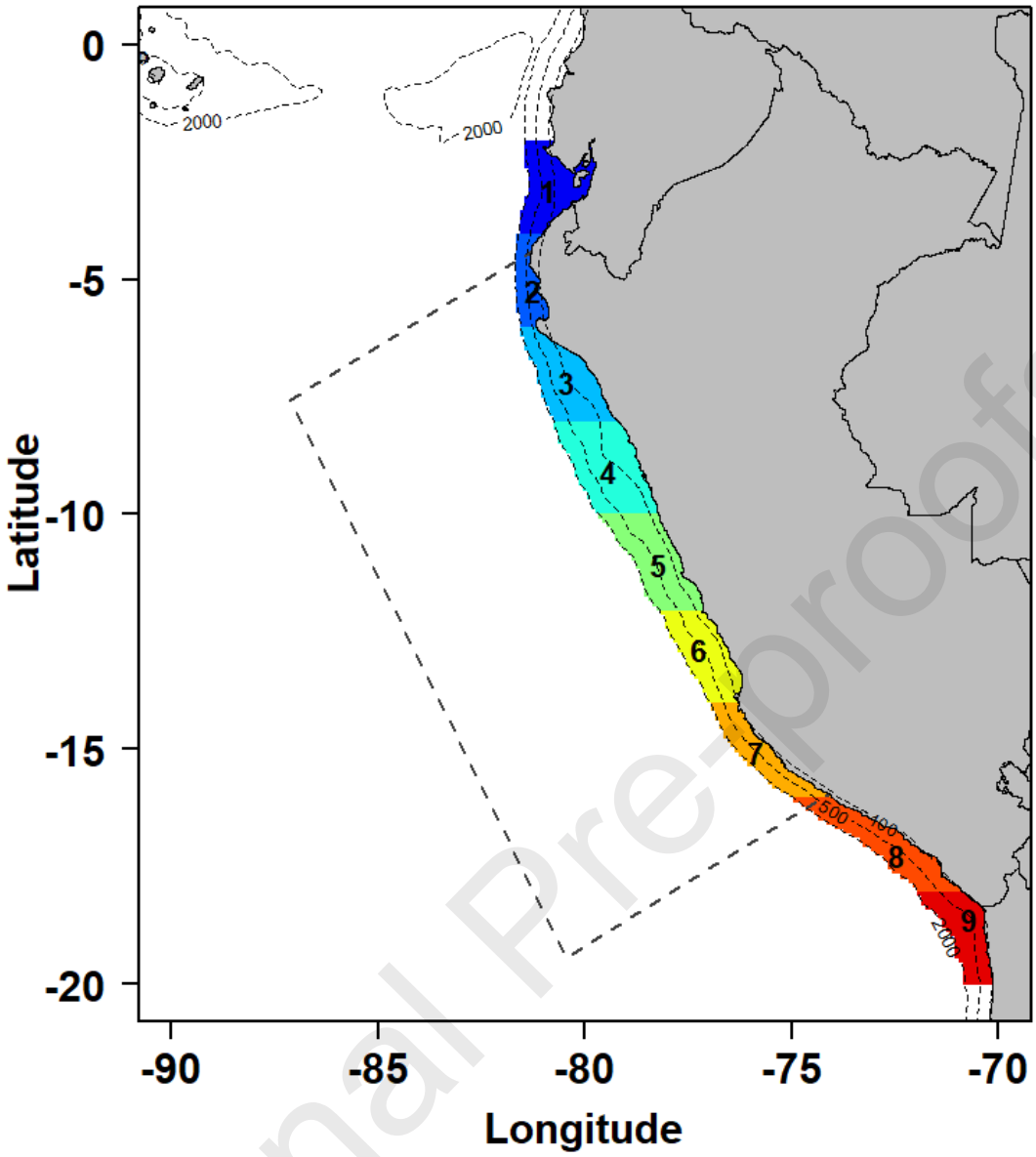

757 Fig. 1 Model domain at 10 km of spatial resolution (D01). The dotted rectangle represents the
758 nested model domain (D02) at 2 km resolution. Spawning areas (1 to 9) are every 2 degrees of
759 latitude between 2º S and 20º S. Three isobaths (100 m, 500 m and 2000 m) are shown.

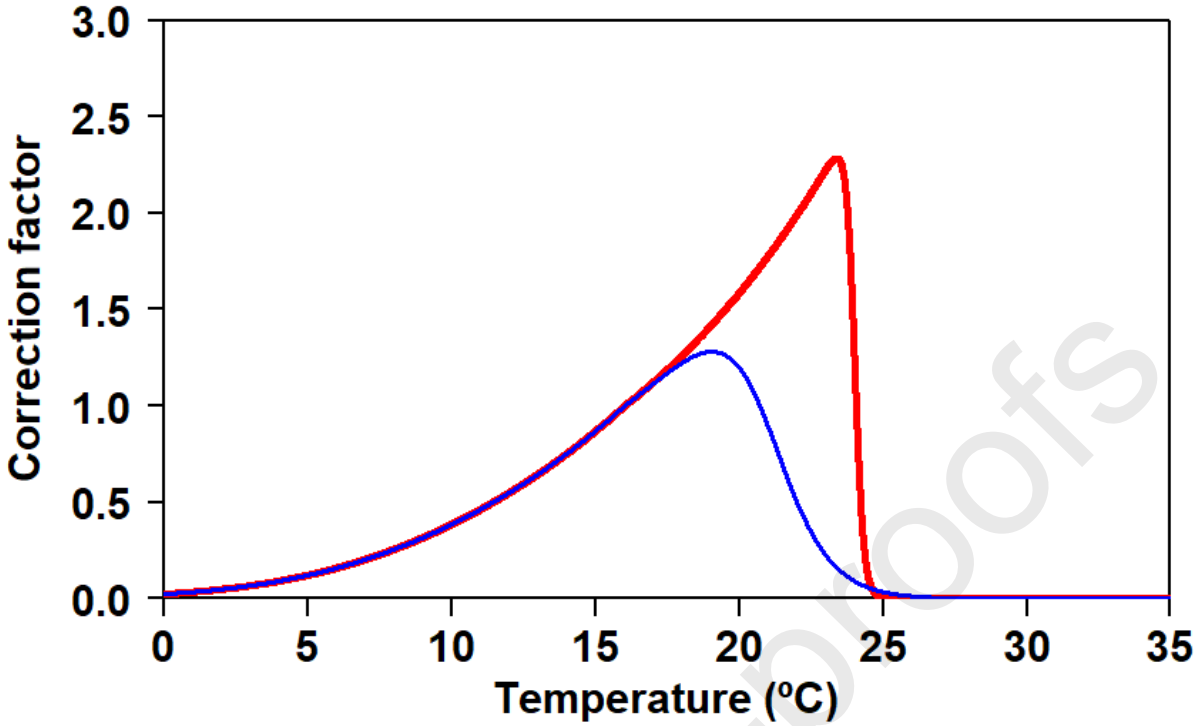

Fig. 2 Temperature correction curves for the metabolic flux in the dynamic energy budget model (equation 5); blue and red curve correspond respectively to case 1 and case 2 in Table 1.

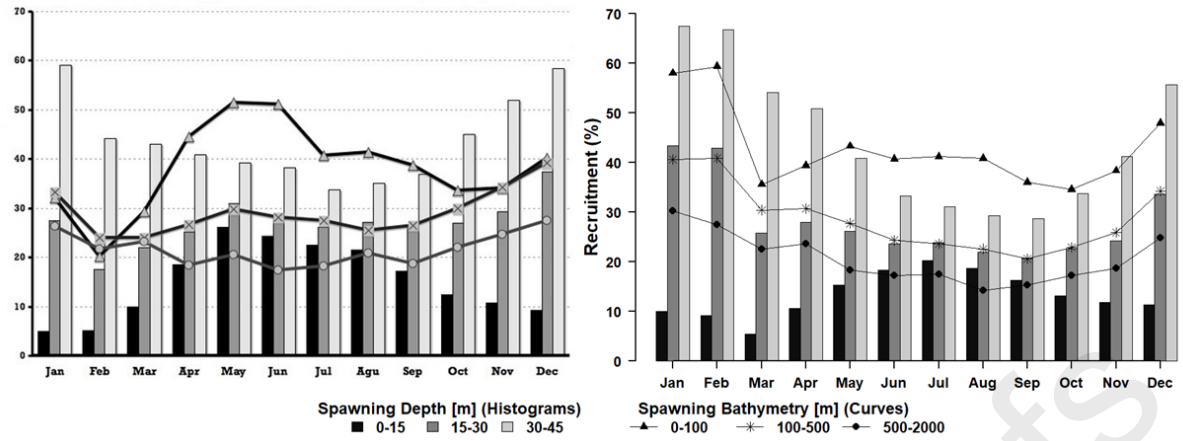

Fig. 3 Percentage of recruited larvae of Peruvian anchovy obtained for different spawning months, spawning depths, and isobaths delimiting spawning areas horizontally from (Brochier et al. (2008) (left) and from Sim 4 (right).

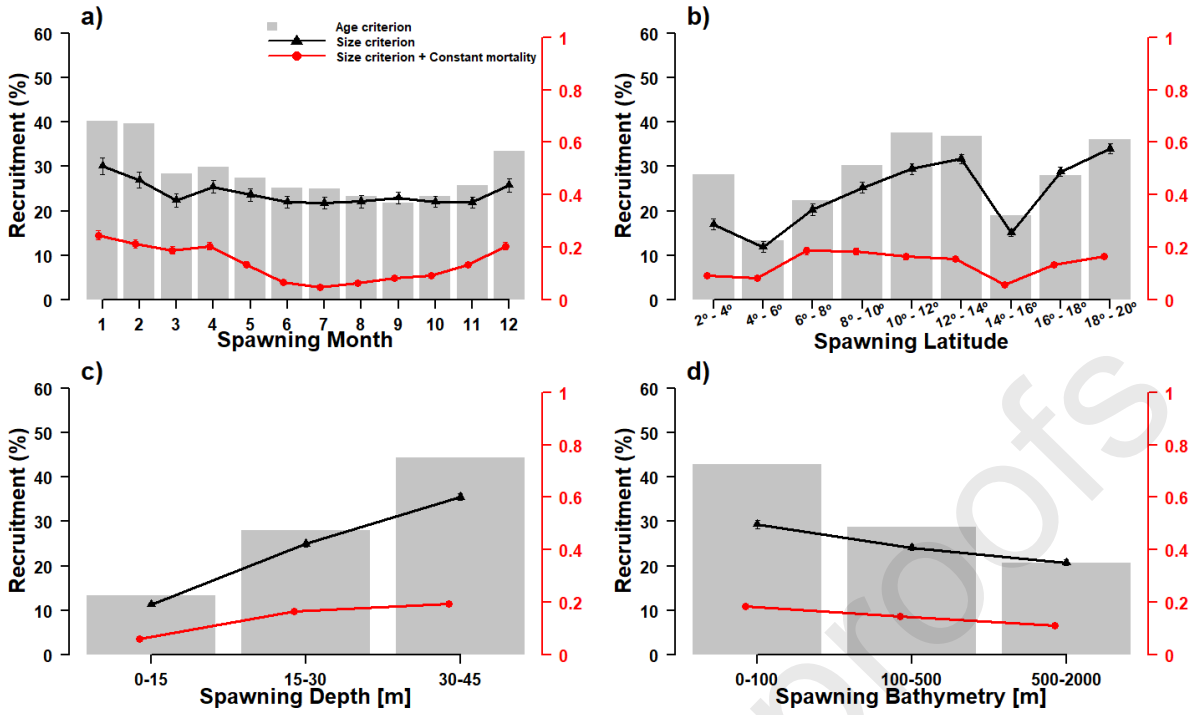

Fig. 4 Percentage of recruited larvae of Peruvian anchovy obtained for different a) spawning months, b) spawning latitudes, c) spawning depths and d) isobaths delimiting spawning areas horizontally using different criteria for recruitment (size criteria -black lines-, size criteria plus constant daily mortality -red lines-) in Sim 5. Recruitment values based on age criteria -grey bars- were taken from Sim 4.

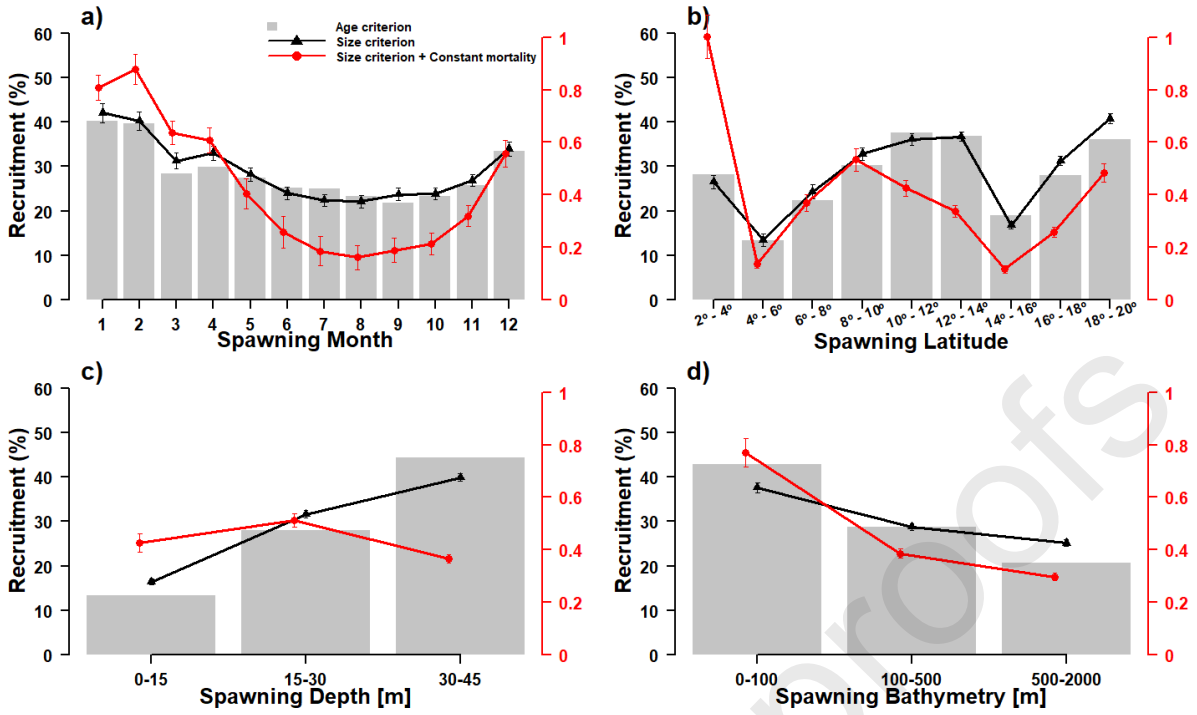

Fig. 5 Same as Fig. 4 in Sim 6.

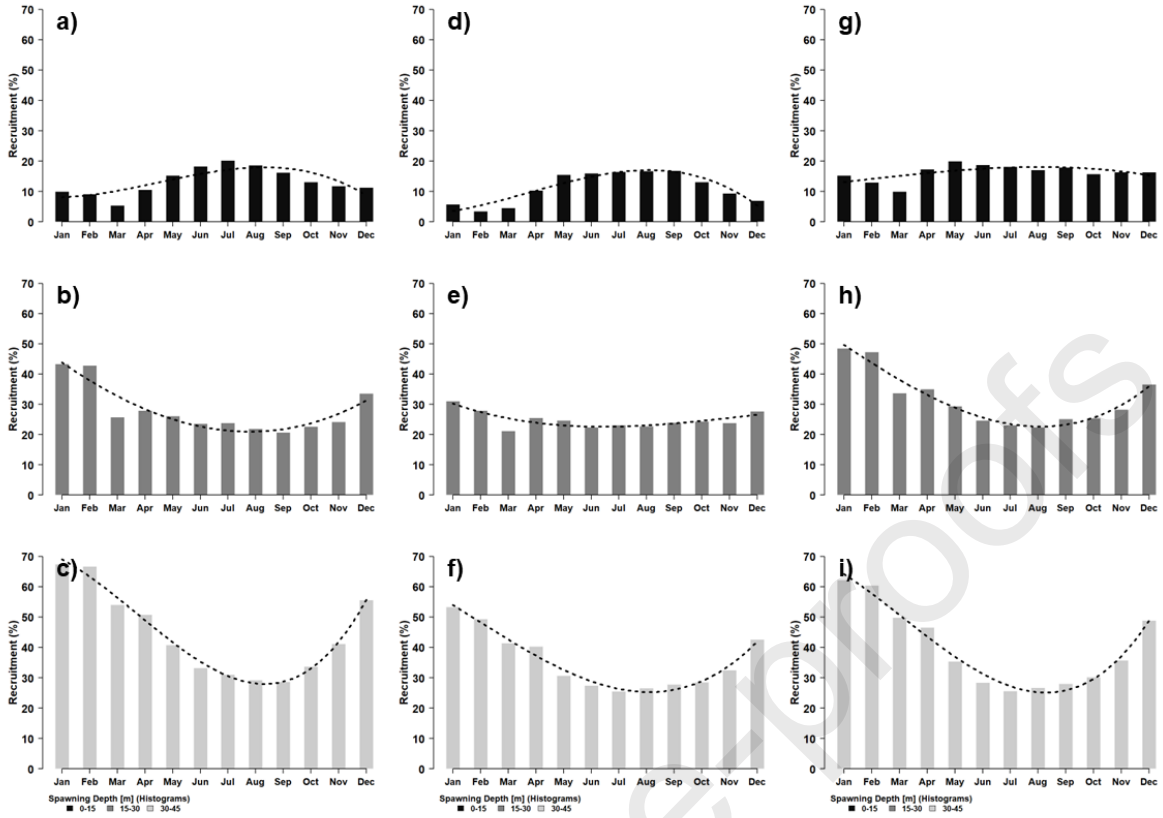

Fig. 6 Percentage of recruited larvae of Peruvian anchovy obtained for different spawning depths in Sim 4 criterion 1 (a, b, c), Sim 5 criterion 2 (d, e, f) and Sim 6 criterion 2 (g, h, i). Spawning depth is (a, d, g) 0 - 15 m, (b, e, h) 15 - 30 m, (c, f, i) 30 - 45 m. The dotted curves are third degree polynomial models fitted to the recruitment patterns.

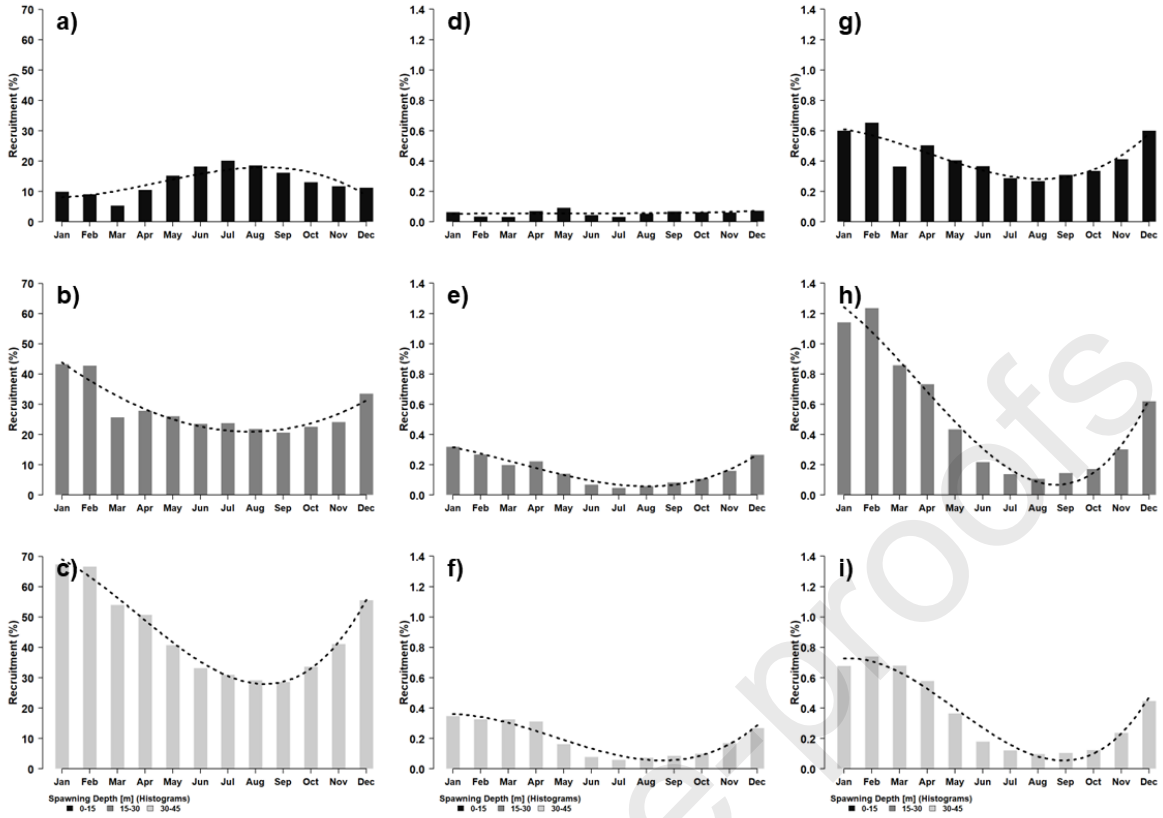

Fig. 7 Same as Fig. 6 but with mortality included in Sim 5 and Sim 6 (criterion 3).

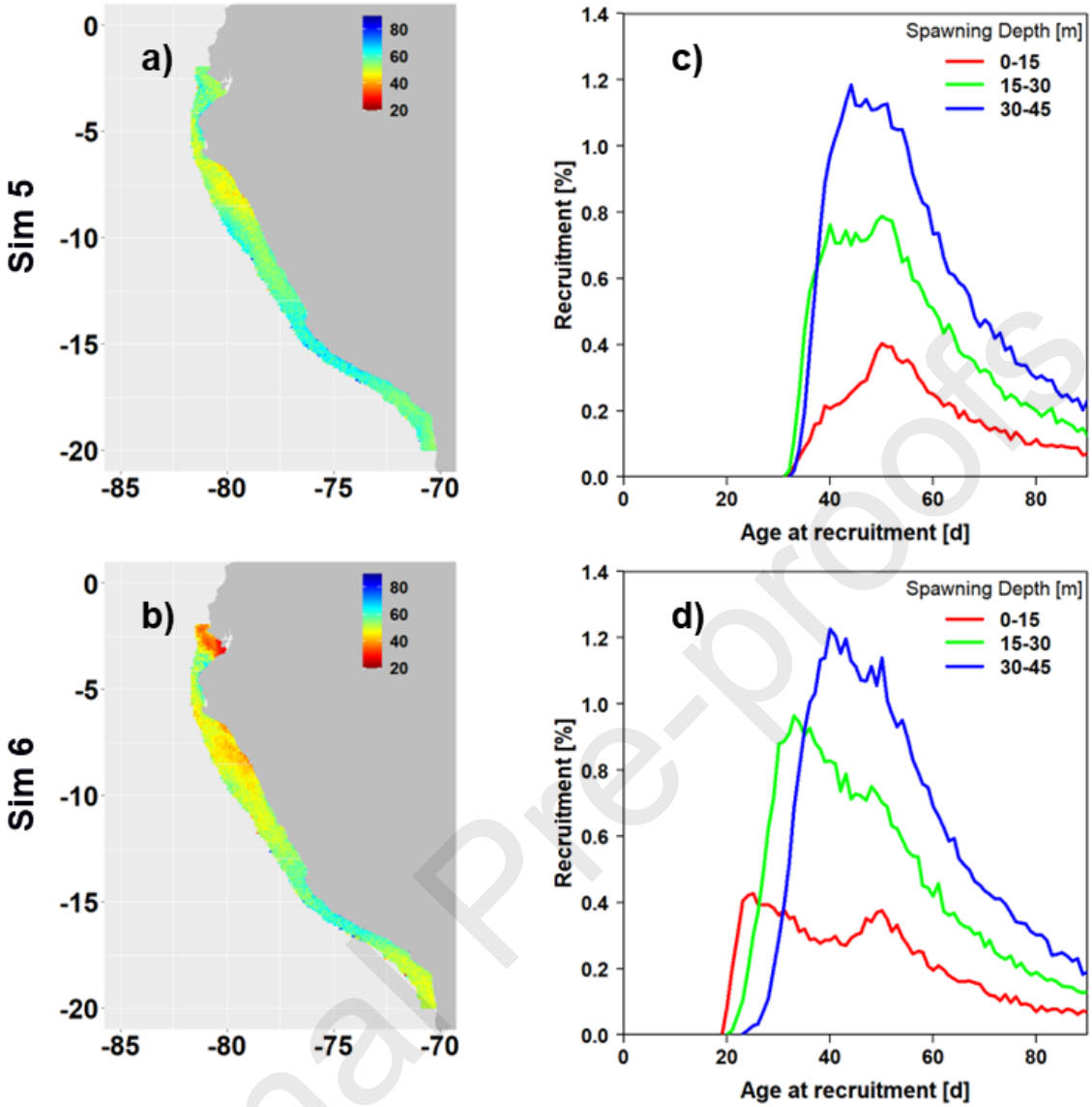

Fig. 8 Spatial distribution of average age at recruitment (a, b) and mean daily recruitment depending on age (c, d), for 0 - 15 m (red line), 15 - 30 m (green line) and 30 - 45 m (blue line) spawning depth. Results obtained with (a, c) Sim 5 and (b, d) Sim 6 using recruitment criterion 2 (no mortality).

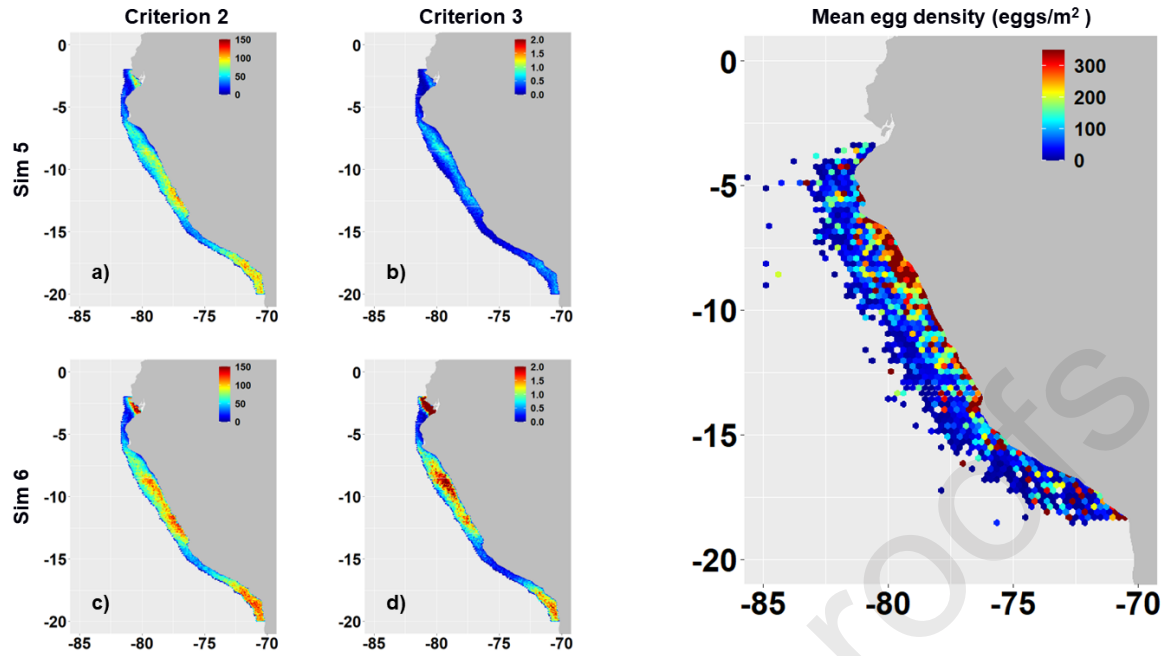

Fig. 9 Spatial distribution of the average number (ind/m^2) of simulated Peruvian anchovy larvae recruiting according to their spawning location obtained with (a, b) Sim 5 and (c, d) Sim 6 using recruitment criterion 2 (no mortality) (a, c) and 3 (with mortality) (b, d). (e) Spatial distribution of Peruvian anchovy mean egg density (eggs/m^2) derived from IMARPE field surveys from year 1961 to 2016. Note that cell grid was 0.1° x 0.1° in a - d and 0.25° x 0.25° in e).

Table 1: Summary of simulations performed to study recruitment predictions sensitivity. This table list all parameters that differ between simulations.

	Sim 1	Sim 2	Sim 3	Sim 4	Sim 5	Sim 6	Sim 7	Sim 8
Figures	S2	S2	S2	3,4,5,6,7, S3	4,6,7,8,9, S4	5,6,7,8,9, S5	S4	S5
Configuration domain	D01	D02s	D02r	D01	D01	D01	D01	D01
Forcing type	physical	physical	physical	physical & biogeochemical	physical & biogeochemical	physical & biogeochemical	physical & biogeochemical	physical & biogeochemical
Bathymetry	STRM30	Interpolated from Sim1	STRM30	STRM30	STRM30	STRM30	STRM30	STRM30
Horizontal grid resolution	10 km	2 km	2 km	10 km	10 km	10 km	10 km0	10 km
Latitudinal spawning range	6º S - 14º S	6º S - 14º S	6º S - 14º S	2º S - 20º S	2º S - 20º S	2º S - 20º S	2º S - 20º S	2º S - 20º S
Growth sub-model	No	No	No	No	Yes	Yes	Yes	Yes
Recruitment criterion evaluated*	1	1	1	1	2 and 3	2 and 3	2 and 3	2 and 3
Correction Temperature**	--	--	--	--	Case 1	Case 2	Case 1	Case 2
Food half saturation constant (K)	--	--	--	--	1.6 $\mu molCL^{-1}$	1.6 $\mu molCL^{-1}$	0 $\mu molCL^{-1}$	0 $\mu molCL^{-1}$
Mortality	--	--	--	--	Yes	Yes	Yes	Yes

*Recruitment criterion 1: retention at 30 days; 2: retention at 20 mm; 3: retention at 20 mm with constant mortality.

**Temperature correction factor case 1: $T_H = 294\ K\ (= 21°C)$ and $T_{AH} = 95\ 000\ K$; case 2: $T_H = 297\ K\ (= 24°C)$ and $T_{AH} = 570\ 000\ K$

760 Table 2: Parameters used for the bioenergetic model describing larval growth. These values
761 were estimated by Pethybridge et al. (2013) for *Engraulis encrasicolus*, except half saturation
762 constant (K), estimated for the current configuration and fixed at 1.6 µmol C L^{-1}. Comparison
763 with data showed that these parameters allowed to reproduce *Engraulis ringens* larval growth.
764 The values of T_L, T_H, T_{AL}, T_{AH} are detailed for case 1 and case 2 respectively (see section 2.7).

Primary parameters (rates are at reference temperature T_1 = 289 K (= 16°C)			
Symbol	Value	Unit	Definition
L_h	0.28	cm	Hatch length
L_b	0.35	cm	Yolk-sac to feeding larva threshold
T_A	9800	K	Arrhenius temperature
T_L	279/279	K	Lower temperature boundary
T_H	294/297	K	Upper temperature boundary
T_{AL}	20 000/20 000	K	Arrhenius temperature for lower boundary
T_{AH}	95 000/570 000	K	Arrhenius temperature for upper boundary
K	1.6	µmol C L^{-1}	Half-saturation constant
κ_X	0.71	-	Fraction of food energy fixed in reserve
$\{\dot{p}_{Xm}\}$	325	J.cm^{-2}.d^{-1}	Maximum surface-specific ingestion rate
$[E_m]$	2700	J cm^{-3}	Maximum reserve density
$[E_G]$	4000	J.cm^{-3}	Volume-specific costs of structure
$[\dot{p}_M]$	48	J.cm^{-3}.d^{-1}	Volume-specific somatic maintenance rate
κ	0.7	-	Fraction of mobilized reserve allocated to growth and somatic maintenance
Auxiliary and Compounds parameters			
Symbol	Value	Unit	Definition
δ_M	0.152	-	Shape coefficient
$\{\dot{p}_{Am}\}$	$\kappa_X\{\dot{p}_{Xm}\}$	J.cm^{-2}.d^{-1}	Maximum surface-area-specific assimilation rate

765
766
767

Declaration of interests

☒ The authors declare that they have no known competing financial interests or personal relationships that could have appeared to influence the work reported in this paper.

☐ The authors declare the following financial interests/personal relationships which may be considered as potential competing interests: